Energy & Buildings 259 (2022) 111843

Contents lists available at ScienceDirect

Energy & Buildings

journal homepage: www.elsevier.com/locate/enb

Unravelling the multilevel and multi-dimensional impacts of building and tree on surface urban heat islands

Jike Chen [a], Peijun Du [b], Shuangen Jin [a,c,*], Haiyong Ding [a], Cheng Chen [d], Yongming Xu [a], Li Feng [e], Guanhua Guo [f], Hongrui Zheng [b], Minmin Huang [a]

[a] School of Remote Sensing & Geomatics Engineering, Nanjing University of Information Science & Technology, Nanjing 210044, China
[b] Key Laboratory for Land Satellite Remote Sensing Applications of Ministry of Natural Resources, Nanjing University, Nanjing 210093, China
[c] Shanghai Astronomical Observatory, Chinese Academy of Science, Shanghai 200030, China
[d] Jiangsu Province Surveying & Mapping Engineering Institute, Nanjing, 210013, China
[e] School of Hydrology and Water Resources, Hohai University, Nanjing, 210098, China
[f] School of Geographical Sciences, Guangzhou University, Guangzhou, 510006, China

ARTICLE INFO

Article history:
Received 5 November 2021
Accepted 5 January 2022
Available online 11 January 2022

Keywords:
Land surface temperature
building
tree
multi-dimensional characteristics
multilevel impact

ABSTRACT

The multilevel effects of landscape composition and configuration on daytime land surface temperature (LST) has been examined. However, how 2D and 3D characteristics of building and tree hierarchically interact to influence LST and how such effects vary diurnally were yet unknown. Using thermal satellite imagery, 2D and 3D characteristics of urban landscapes, and multilevel models (i.e. the random intercept model (RIM) and the random coefficient model (RCM)), we quantified the multi-dimensional and hierarchical effects of buildings and trees on LST as well as their diurnal contrast. Our results showed that combining landscape pattern and 3D urban morphology can capture more of the variation in diurnal LST than using them separately, regardless of single-level ordinary least squares (OLS) and multilevel models. Moreover, the multilevel models performed better than OLS models in explaining the impacts of landscape pattern and 3D urban morphology on LST for both day and night, and the RCM performed better than that the RIM. During the day, the standard deviations of the residual and autocorrelation in the residual for the RCM were 1.315 and 0.131, respectively, but 1.715 and 0.312 for OLS, respectively. Similarly, a smaller autocorrelation in the residual was produced by the RCM (0.155) than by OLS (0.366) at night. The spatial heterogeneity of LST was linked tightly to the percent cover of trees and the largest patch index of tree during the day, but was primarily dominated by the edge density of the buildings and the mean building height at night. Moreover, we found significant differences in the random effects of the composition and 3D urban morphology on the LST at the block level. The random impacts of the percent cover of buildings on both daytime and nighttime LSTs varied most across urban blocks. These findings provide urban planners and researchers a more thorough picture of LST-landscape associations from multi-dimensional and multilevel perspectives.

Introduction

Owing mainly to the replacement of natural with artificial land surfaces and population increase, rapid urbanization is seriously affecting the Earth's systems, and has induced a series of problems related to urban environment ([1,2]). The urban heat island (UHI), in which higher temperature was found in urban area compared to its peripheral rural environments. One of these well-known primary concerns is urban heat island (UHI), in which higher temperatures are found in urban areas than in their peripheral rural environments ([3]). In these areas, the enhanced heat stress caused by UHI effects has profound impacts on energy consumption ([4,5]), plant phenology ([6,7]), and even mortality risk ([8]). As a result, strategies to mitigate UHI effects are crucial to enhance a city's resilience to climate change.

Urban land cover has been regarded as a fundamental surrogate for exploring how landscape heterogeneity impacts variations in LST ([9–11]). Previous studies concentrated largely on the impacts of the 2D and 3D characteristics of vegetation and impervious surfaces on LST, by using a regular grid as the analytical unit ([12–14]). Two-dimensional characteristics are usually represented by landscape pattern, including composition and configuration (e.g., shape, edge, and aggregation) ([15]). It is generally recognized that

* Corresponding author.
E-mail addresses: sgjin@nuist.edu.cn, sgjin@shao.ac.cn (S. Jin).

https://doi.org/10.1016/j.enbuild.2022.111843
0378-7788/

an increase in the tree canopy fraction can lead to a reduction in both daytime and nighttime LSTs ([16,17]), whereas building surface coverage contributed to urban warming. Moreover, LST can be significantly affected by the spatial configuration of buildings and trees, but the magnitude, significance, and even direction varied in previous studies ([18–20,16]). Furthermore, several previous studies have implied that the 3D characteristics of urban morphology played important roles in influencing the urban thermal environment ([21–23]). These studies can be categorized into two categories: Firstly, some researchers adopted micro-climate numerical models to investigate the impact of the surrounding micro-environment on urban micro-climate ([24–27]). The findings from such studies provide a feasible method to provide effective UHI mitigation strategies. However, they failed to guide urban planning and design at the city level because of the specific materials and elements used in micro-thermal research ([28]). Secondly, few studies have tried to explore the impacts of 3D building and tree structures on urban LST at the city level. It suggested that when the mean vegetation height at a 30 m grid increased from 0-2 m to 20-22 m, daytime LST decreased by 4.10 °C ([29]). The 2D characteristics of urban landscapes were found to affect daytime LST more than the 3D urban morphology in China and the United States ([17,30,31]), which contrasts with the findings of research conducted in Iran ([32]).

Although the relationships between urban landscapes and LST have previously been explored with grid units, several limitations to such studies need to be acknowledged. First, despite UHI effecting involving multilevel interacting processes ([33–35]), the hierarchical structure of their explanatory variables has been ignored. Landscape composition, configuration, and 3D urban morphology variables should be used at different levels. This is because the composition and 3D urban morphology represent features that do not consider the spatial characteristics of patches. In contrast, configuration is used to measure the spatial arrangement of land cover patches and offers contextual knowledge for composition metrics ([15]). In a previous study, configuration metrics were found to explain more of the variation in daytime LST than composition metrics, where the individual pixels and cluster-derived groups were separately used as level-1 and level-2 units ([36]). A dense and continuous tree configuration at the administrative ward level seems to enhance the cooling effect of the dissemination-area-level tree canopy fraction ([37]), when the administrative ward was subdivided into smaller nested dissemination areas.

In addition, the irregular urban forms at the neighborhood scale prevents the grid unit from fully characterizing the structure-function boundaries of the city, which may produce biased estimates of the effects of buildings and trees on the thermal environment ([30]). The neighborhood scale is regarded as an appropriate and operational scale for urban development projects and the implementation of urban sustainability measures. The urban blocks has usually been taken as the analytical unit to describe the neighborhood scale in recent UHI research, because they indicate the thermal advection at the neighborhood scale ([38–41]). For instance, some case studies have adopted urban blocks as statistical units to investigate the impact of 3D building structure, composition and configuration of vegetation on daytime LST ([42,22,43]).

Even though the multilevel impacts of landscape composition and configuration on LST have been examined during the day, how landscape pattern and 3D urban morphology hierarchically interact to influence LST together with diurnal contrast is not yet understood. Moreover, to date, no study has attempted to elucidate the varying local effects of composition and 3D urban morphology metrics across different urban blocks, while simultaneously allowing for pixel-level and urban block-level effects. These research gaps inspired us to systematically examine the relationships between urban landscapes and diurnal LST from multilevel and multi-dimensional perspectives. The three key objectives to be achieved in this study were as follows: (1) to examine whether the inclusion of 3D urban morphology could improve the performance of both single-level and multilevel models, and to compare the performances of these approaches; (2) to discriminate the dominant factors influencing LST variation for both day and night, when the multilevel and multi-dimensional impacts of urban landscapes are considered; and (3) to examine how the responses of diurnal LST to composition and 3D urban morphology indicators vary with urban blocks. The results from this work provide fresh insights into whether multilevel model are better than single-level models to explain LST variation during both day and night, and how landscape pattern and 3D urban morphology metrics hierarchically impact LST as well as their day-night contrast.

Materials and methods

Study area

In this research, we concentrated on the city of Nanjing, the capital of Jiangsu Province, China (Fig. 1 (a)). The city has subtropical monsoon climate, with a mean daily high temperature of 28.6 °C in July, being widely known as one of China's "Four Furnace" ([44]). Nanjing has witnessed a rapid rate increase in urbanization since the early 2000s: the built-up area increased from 153.81 km^2 in 2000 to 726.4 km^2 in 2012 ([45]). The number of hot days, when the air temperature is over 35 °C, was relatively high in the 1950s (16.2 days/year) and the 1960s (18 days/year) in Nanjing, and were relatively low from the 1970s (13.3 days/year) to the 1980s (9.7 days/year). However, Nanjing has tended to experience more hot days since the 1990s. The average number of hot days was 18.4 days/year from 2001 to 2007 ([46]). Nanjing has a heterogeneous land-use composition, including buildings, trees, grasses, commercial, industrial, bare soil and open water. Such characteristics make Nanjing city an ideal area to explore the effects of landscape pattern and 3D urban morphology on LST. Our study area is located in central Nanjing, encompassing approximately 205 km^2. The study area was selected mainly owing to the availability of LiDAR data, which are necessary to quantify 3D urban morphology.

Data sources

Land cover classification

To characterize landscape pattern and 3D urban morphology, we need detailed information on urban land cover. In this study, we combined an IKONOS-2 image and airborne LiDAR data to map urban land cover with a Random Forest classifier using an object-based method. Airborne LiDAR data, with a point density of approximately 4.1 $points/m^2$, were acquired on April 21 and 22, 2009. To ensure the date of the IKONOS-2 image as close as possible to the acquisition time of airborne LiDAR data, we checked all the available IKONOS-2 images according to acquisition date and cloud cover. As a result, we used the IKONOS-2 image on June 18, 2009. IKONOS-2 images includes four spectral bands (blue, green, red, and near-infrared) with 3.2 m spatial resolution.

We classified urban land cover into seven classes, buildings, trees, roads, grass, water, cropland and bare soil, with a 99.35% overall accuracy and 3.2 m spatial resolution, as is shown in Fig. 1 (c). Given the availability of vertical structures, we considered two classes (buildings and trees) in this study. The user's accuracies of buildings and trees were 99.0% and 99.13%, respectively, and 99.35% and 98.85% producer's accuracies were obtained for buildings and trees, respectively.

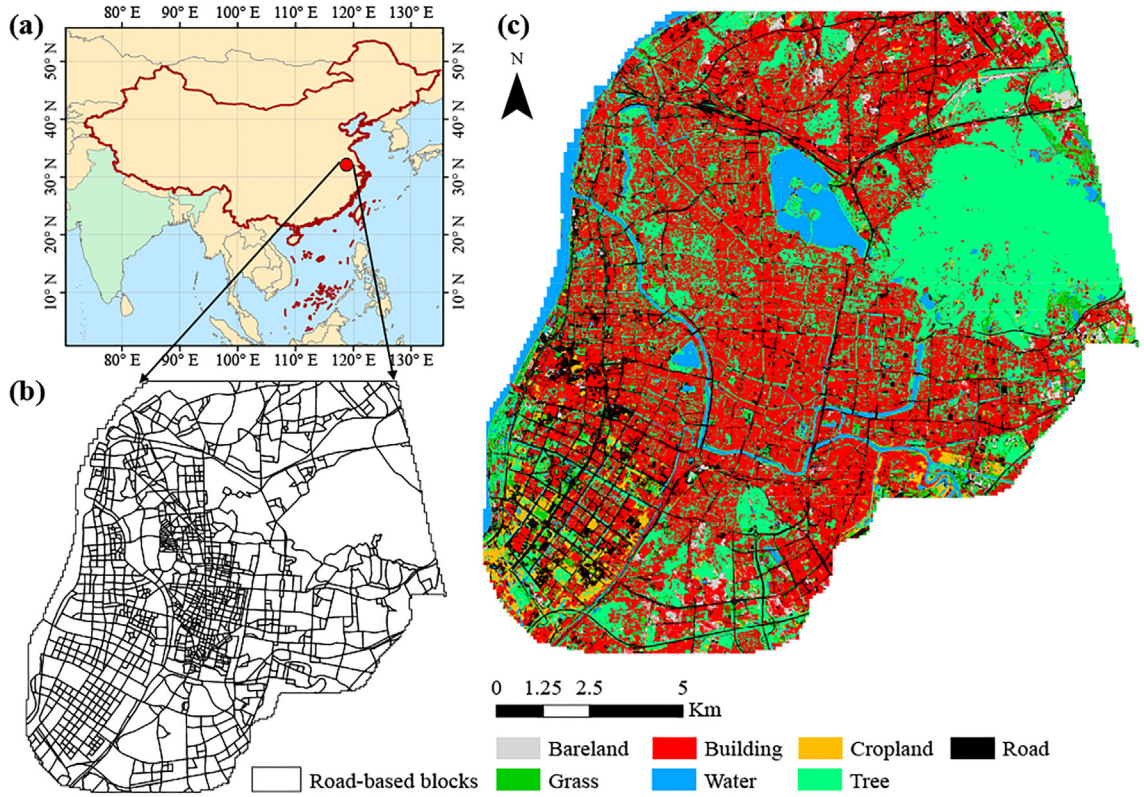

Fig. 1. (a) Location of Nanjing city in China; (b) Road-based blocks in the study area; (c) Land cover map which was obtained by combining airborne LiDAR and IKONOS-2 image.

Land surface temperature

The diurnal LST data were acquired from the Advanced Spaceborne Thermal Emission and Reflection Radiometer (ASTER) surface kinetic temperature product (AST_08), which has a pixel size of 90 m ([47]). The AST_08 product was produced using five thermal infrared channels ranging from 8 to 12 μm. When deriving ASTER LST, the temperature/emissivity separation (TES) technique was first used to estimate the emissivity values. Next, by adopting Planck's law with the emissivity values, the ASTER surface kinetic temperature was determined. More detailed information about the computation of ASTER LST can be found in a previous study ([48]). The absolute accuracy of ASTER LST is within $\pm$1.5 K ([47,48]).

To ensure the date of the LST data coincided with the acquisition time of urban land cover as closely as possible, daytime ASTER LST data on May 11, 2011 (11:00 a.m.) was selected, whereas nighttime LST image was obtained about five hours and six minutes after sunset on April 4, 2011 (22:19 p.m.). The azimuth angles, which are formed by the meridian at the ASTER scene center and the along-track direction, were 9.67° and 170.33° for daytime and nighttime LSTs, respectively. The pointing angles of the ASTER thermal infrared sensor for day and night were 8.57° and −8.56°, respectively. Furthermore, ASTER surface kinetic temperature data were converted to surface temperature in degrees Celsius, and the urban land cover map and ASTER LST data were co-georeferenced.

The 2D and 3D influencing factors

Pixel-level variables

As 3D urban morphology, which is similar to landscape composition, does not consider the spatial arrangement of land cover patches, we quantified composition and 3D urban morphology as level-1 explanatory variables (Fig. 2). In this work, individual pixels of 90 ×90 m (i.e., the same pixel size as LST) were defined as level-1 analytical units. Urban land cover data were resampled to grids of 3 ×3 m. We applied a window with a size of 90 ×90 m to the 3 m urban land cover to compute the composition and 3D urban morphology metrics.

We chose two composition metrics to measure the percent cover of buildings (PER_Build) and trees (PER_Tree) within each pixel. In addition, to concentrate on the 3D urban morphology, we calculated seven types of metrics such as mean height and height variation, to quantify the vertical structures of the buildings and trees (Table 1). These metrics were calculated using land cover, the LiDAR-derived digital surface model (DSM), and the normalized digital surface model (nDSM). The DSM represents the height of earth's surface above the mean sea level, whereas nDSM provides the height distribution of above-ground surface features. We selected these metrics because their potential influence on LST. For example, the sky view factor (SVF) represents the ratio of the visible sky area to the total sky area in one location, and is a key factor in influencing the loss of solar radiation ([49,50]). The average height of buildings and trees (BH_Mean and TH_Mean, respectively) could have an important impact on the urban thermal environment mainly by providing shadows and changing urban surface roughness ([23,51]). Moreover, we considered the influence of topography on LST when quantifying 3D urban morphology, such as the 10th percentile value of DSM-derived building height (BH_P10).

Urban block-level variables

To derive higher-level influencing factors from landscape configuration metrics, we considered urban blocks as level-2 units. The boundaries of the urban blocks were defined as urban streets. We acquired road network data from Nanjing Institute of Surveying, Mapping & Geotechnical Investigation, and OpenStreetMap

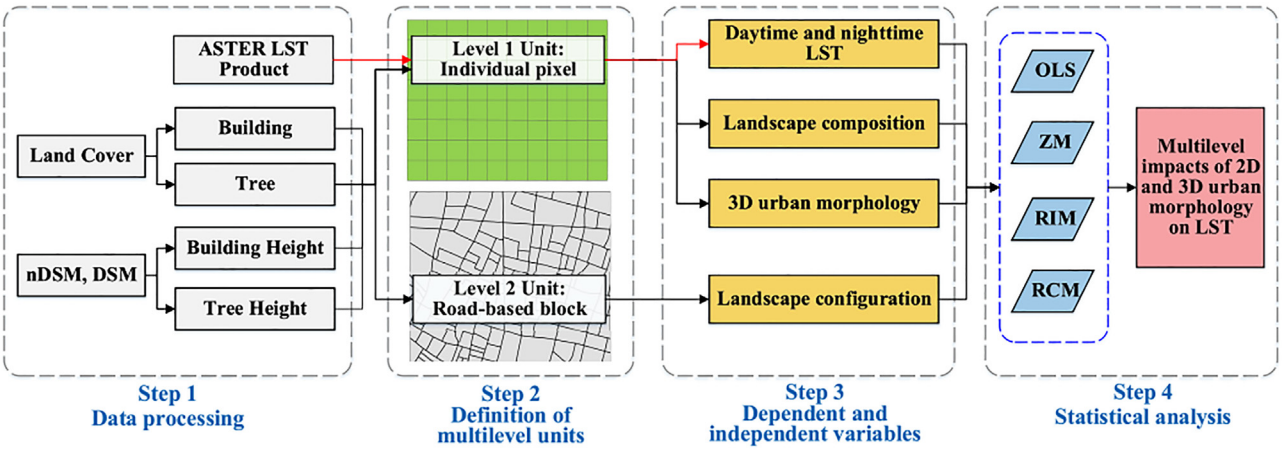

Fig. 2. The conceptual framework of exploring the relationship between LST and landscape pattern and 3D urban morphology with multilevel regression analysis. OLS denotes single-level ordinary least square. ZM represents zero model. RIM and RCM are multilevel models, and indicates random intercept model and random coefficient model, respectively.

Table 1
Descriptive statistics of 2D and 3D urban morphological variables used in this research.

Categories of metrics	Metrics	Definition of metrics
Pixel-level metrics		
Composition	PER_Build, PER_Tree	Proportional abundance of building or tree within each pixel.
3D urban morphology	BH_Max, TH_Max	Maximum building or tree height within each pixel.
	BH_Mean, TH_Mean	Mean height of building or tree within each pixel.
	NBH_SD, NTH_SD	Normalized variance of building or tree height, the ratio of variance to mean of building or tree height.
	BH_P10, TH_P10	The 10th percentile value of DSM-derived building or tree height within each pixel.
	BH_P90, TH_P90	The 90th percentile value of DSM-derived building or tree height within each pixel.
	SVF	The value of sky view factor within each pixel.
Block-level metrics		
Configuration	AREA_SD_BT	Standard deviation in patch area for both building and tree.
	SHAPE_SD_BT	Shape index, which describes the standard deviation in the complexity of landscape including both building and tree.
	CONTAG_BT	Contagion index, measuring the extent to which patches of building and tree are clumped.
	SHDI_BT	Shannon's diversity index, a measure of diversity in community ecology.
	PD_Build, PD_Tree	Density of building or tree patches.
	ED_Build, ED_Tree	The total lengths of all building or tree patches per hectare.
	LPI_Build, LPI_Tree	The area proportion of the largest building or tree patch.
	SHAPE_MN_Build, SHAPE_MN_Tree	The mean shape index of building or tree patches.
	COHESION_Build, COHESION_Tree	Physical connectivity of building or tree patches.

([52]), which were then used to divide the whole study area into irregular urban blocks.

Building and tree patches that overlapped with these urban blocks, were employed to quantify landscape configuration. Based on the theoretical importance and applicability as well as their association with LST ([19,53–55]), we selected nine commonly used configuration metrics at both the class and landscape levels (Table 1). To quantify the spatial configuration of buildings or trees in every urban block, we used class-level metrics, including patch density (PD), edge density (ED), largest patch index (LPI), mean shape index (SHAPE_MN), and patch cohesion index (COHESION). In contrast, over all patches of buildings and trees, we computed landscape-level metrics, which consisted of standard deviation in patch area (AREA_SD), standard deviation of shape index (SHAPE_SD), contagion index (CONTAG), and Shannon's diversity index (SHDI).

Multilevel regression model

Because the factors influencing LST were hierarchically structured in this study, the commonly used ordinary least squares (OLS) model would fail to fully explain potential sources of error variance ([36]). As a result, we used multilevel regression models to simultaneously reveal the effects of composition, 3D urban morphology and configuration on LST at both the pixel and block levels. The multilevel regression models were built using the following steps ([56–58]).

Step 1: First, we built an empty multilevel regression model (i.e., zero model (ZM)), and calculated the intra-class correlation coefficient (*ICC*). The *ICC* value was used to measure the degree of LST variation, resulting from the differences between urban blocks. The empty model can be reformulated as follows:

$$Y_{ij} = \beta_{0j} + e_{ij} \quad (1)$$

$$\beta_{0j} = \alpha_{00} + u_{0j} \quad (2)$$

$$e_{ij} = N(0, \sigma_e^2) \quad (3)$$

$$u_{0j} = N(0, \sigma_{u_0}^2) \quad (4)$$

where Y_{ij} is the estimated value of LST in pixel i within block j. α_{00}, the so-called "fixed intercept", is the grand mean of intercept, and u_{0j}, the so-called "random intercept", is the difference for each urban block between its intercept and α_{00}. e_{ij} is the residual error

of pixel-level. σ_e^2 and $\sigma_{u_0}^2$ denote the variances of pixel-level and block-level errors, respectively. Moreover, they are assumed to be normally distributed and independent of each other. In order to explore whether LST varies among different urban blocks, *ICC* is computed as follows:

$$ICC = \frac{\sigma_{u_0}^2}{\sigma_{u_0}^2 + \sigma_e^2} \quad (5)$$

The ICC value ranges from 0 to 1, in which the larger the value of ICC is, the more LST variation can be attributed to the block-level.

Step 2: Adding the influencing factors at both pixel-level and block-level to the empty model, the model, called random intercept model (RIM) can be expressed as follows:

$$Y_{ij} = \beta_{0j} + \beta_1 x_{ij} + e_{ij} \quad (6)$$

$$\beta_{0j} = \alpha_{00} + \alpha_{01} z_{ij} + u_{0j} \quad (7)$$

where x_{ij} represents influencing factors of LST in the pixel-level, which include landscape composition and 3D urban morphology, while z_{ij} denotes landscape configuration metrics in the block-level. The regressed estimates of β_1 and α_{01} are the slopes of influencing variables in the pixel-level and block-level, respectively.

Step 3: Incorporating the random effects of items on the slopes of explanatory variables into the RIM model can create the random coefficient model (RCM):

$$Y_{ij} = \beta_{0j} + \beta_{1j} x_{ij} + e_{ij} \quad (8)$$

$$\beta_{0j} = \alpha_{00} + \alpha_{01} z_{ij} + u_{0j} \quad (9)$$

$$\beta_{1j} = \alpha_{10} + u_{1j} \quad (10)$$

where α_{10}, the so-called "fixed slope", is the fixed effects of explanatory variables in the pixel-level on LST. u_{1j}, the so-called "random slope", represents the random effects of these explanatory variables, indicating the extent to which the slopes of explanatory variables in the urban block *j* vary around α_{10}.

Statistical analysis

To clarify the impacts of urban landscapes on LST from both multilevel and multi-dimensional perspectives, two scenarios were introduced to construct models: (1) LST - landscape pattern (composition and configuration), (2) LST - landscape pattern and 3D urban morphology (composition, 3D urban morphology and configuration). In this work, we built a single-level OLS model as the reference. Multilevel models were utilized to reveal the hierarchical effect of influencing factors on LST. ZM was executed to check the necessity of using multilevel regression model. When exploring the effects of building and tree on LST, RIM allowed the intercept to differ across road-based blocks. RCM aimed to evaluate the fixed and random effects of composition and 3D urban morphology metrics on LST. When landscape pattern was used as independent variables, composition and configuration metrics were defined as level-1 and level-2 variables for multilevel model, respectively. While expressing LST as a function of landscape pattern and 3D urban morphology with multilevel model, level-1 variables included composition and 3D urban morphology metrics, and configuration metrics were considered as level-2 variables.

All pixel-level and block-level variables were grand mean-centered, and scaled by the corresponding standard deviations before the regression. These treatments are of great help to eliminate convergence problems during the estimation of regression coefficients. Variance inflation factor (VIF) vale for each influencing factor, together with Pearson correlation coefficient, were consulted to test the potential multicollinearity among explanatory variables. As a general rule, it is indicated that the value of VIF should be less than 7.5 ([59]). As a result, VIF values in all models were less than 7.5 during the day, when BH_P10, BH_P90, TH_P10, SVF and CONTAG_BT were excluded. At night, BH_P90, TH_P10, TH_P90, SVF and CONTAG_BT were excluded.

Considering the limitation of R^2 to evaluate the goodness of multilevel model ([60]), we presented Akaike Information Criterion (AIC) and Root mean square error (RMSE) as the model comparison tools. Moreover, we calculated Moran's I index (Moran's I) to weigh the spatial autocorrelation of the residual ([61]). A positive Moran's I value demonstrates spatial clustering of the residual in adjacent locations, and a value of 0 suggests perfect randomness of the residual. Generally, smaller values of AIC, RMSE and Moran's I suggest better performance of the regression models. In this work, the best regression models were selected to evaluate the multilevel impacts of landscape pattern and 3D urban morphology on LST. The relative contribution of each explanatory variable was measured by standardized regression coefficients.

Results

Effects of landscape pattern and 3D urban morphology on LST revealed by single-level model

We first applied a single-level OLS regression model to quantify the impacts of buildings and trees on LST. During the day, the explanatory power (i.e., adjusted R^2) of the OLS model with landscape pattern was 36.7%, and the inclusion of 3D urban morphology in this model explained 4.6% more of the variation in daytime LST. As shown in Fig. 3 (a) and Fig. 4 (a), the AIC and RMSE values suggested that the OLS model considering landscape pattern and 3D urban morphology performed more accurately than the OLS model only considering landscape pattern. According to the Moran's I values of the residuals, a smaller autocorrelation was produced by the combination of landscape pattern and 3D urban morphology than by landscape pattern alone (Table 2).

From the data in Table 4, compared to the 3D urban morphology and configuration variables, composition metrics had stronger correlations with daytime LST. The percent cover of buildings (PER_Build) had a positive effect on daytime LST, whereas the percent cover of tree (PER_Tree) was negatively correlated with daytime LST. In addition, PER_Build was more strongly correlated with daytime LST than PER_Tree. All 3D urban morphology variables, except mean tree height (TH_Mean), exerted significant effects on daytime LST. Shannon's diversity index (SHDI_BT) had a stronger relationship with daytime LST when compared to other configuration metrics.

At night, the OLS model with landscape pattern only explained 21.2% of the variation in LST, but 32.0% of the LST variation was captured by jointly considering landscape pattern and 3D urban morphology. By incorporating 3D urban morphology in the OLS model with landscape pattern, AIC and RMSE values decreased from 68,670 and 1.46 to 65,895 and 1.36, respectively, and the Moran's I value of the residual decreased by 0.08. All explanatory variables, except tree cohesion (COHESION_Tree), were significantly correlated with nighttime LST. PER_Build and PER_Tree had negative impacts on nighttime LST. The mean building height (BH_Mean) was the 3D urban morphology variable most strongly associated with nighttime LST. Regarding configuration metrics, the largest patch index of tree (LPI_Tree) and edge density of trees (ED_Tree) were the two most important determinants of nighttime LST. ED_Tree showed a positive effect on nighttime LST, suggesting that LST increased with an increase in tree edge density.

Although the OLS model with landscape pattern and 3D urban morphology provided a better model fit, we observed significant Moran's I values and gradual changes in the residuals for both day-

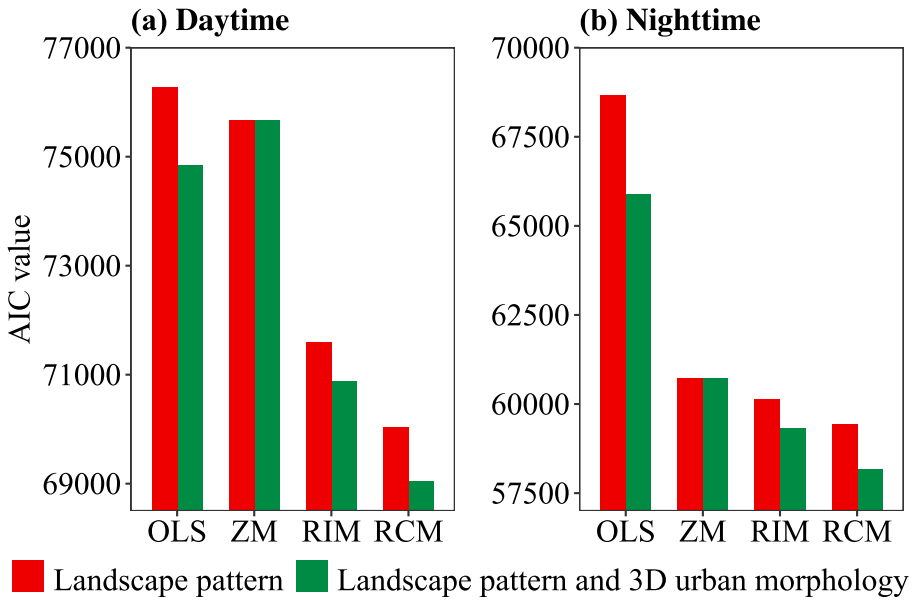

Fig. 3. AIC values of four regressed models with landscape pattern and 3D urban morphology for both (a) daytime and (b) nighttime LSTs.

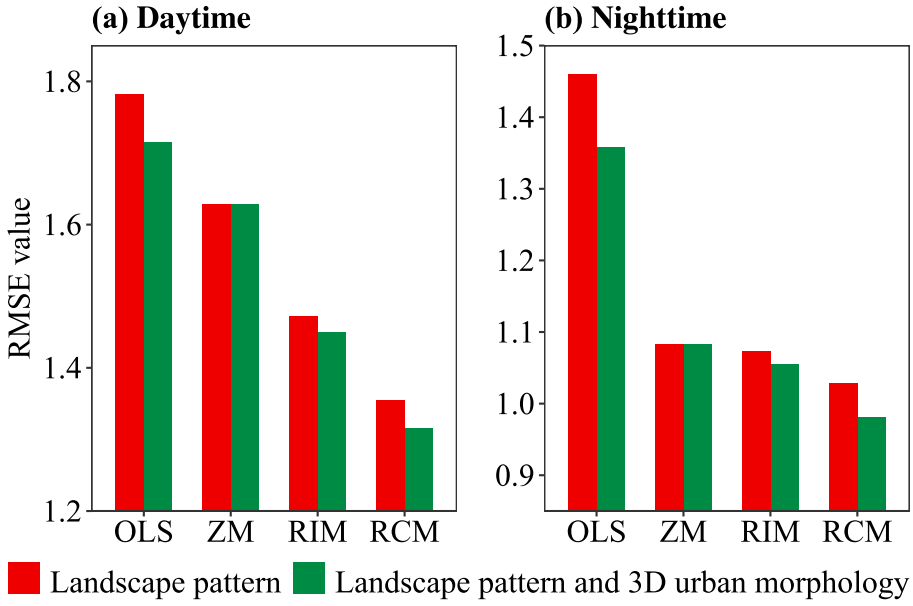

Fig. 4. RMSE values of four regressed models with landscape pattern and 3D urban morphology in terms of (a) daytime and (b) nighttime LSTs.

Table 2
Residual Moran's I of four regressed models for daytime LST.

Model		Residual Moran's *I*		SD of the residuals	
		Level-1	Level-2	Level-1	Level-2
Regression models with landscape pattern	OLS	0.347**		1.782	
	ZM	0.203**	0.248**	1.628	1.068
	RIM	0.158**	0.207**	1.472	0.799
	RCM	0.140**	0.192**	1.354	0.692
Regression models with landscape pattern and 3D urban morphology	OLS	0.312**		1.715	
	ZM	0.203**	0.248**	1.628	1.068
	RIM	0.152**	0.153**	1.449	0.699
	RCM	0.131**	0.130**	1.315	0.573

** represents the significance at 0.01 level (2-tailed)

Table 4
Regressed results of single-level and multilevel models for both day and night.

Variable	Daytime				Nighttime			
	OLS	ZM	RIM	RCM	OLS	ZM	RIM	RCM
Pixel-level effects								
Intercept	30.83**	31.28**	30.89**	31.09**	9.053**	9.492**	9.13**	9.278**
PER_Build	0.675**		0.599**	0.322**	-0.309**		-0.252**	-0.258**
PER_Tree	-0.506**		-0.499**	-0.486**	-0.256**		-0.278**	-0.208**
BH_Max	0.1**		0.042	0.007	-0.068**		-0.031	0.038
BH_Mean	-0.406**		-0.297**	-0.339**	0.412**		0.225**	0.279**
NBH_SD	-0.244**		-0.141**	-0.167**	0.19**		0.102**	0.06**
BH_P10					-0.223**		-0.037**	-0.007
TH_Max	-0.099**		-0.015	-0.028	0.174**		0.107**	0.064**
TH_Mean	-0.042		-0.027	-0.028	0.115**		0.057**	0.04*
NTH_SD	0.118**		0.036*	0.045**	-0.073**		-0.05**	-0.034**
TH_P90	-0.208**		-0.207**	-0.19**				
Block-level effects								
AREA_SD_BT	-0.109**		-0.404**	-0.036	0.243**		0.143	0.152
SHAPE_SD_BT	0.039		0.03	-0.026	-0.259**		-0.201**	-0.172**
SHDI_BT	0.412**		0.151*	0.121	-0.422**		-0.057	-0.004
PD_Build	-0.01		0.069	0.038	0.072**		0.025	-0.004
ED_Build	-0.077*		-0.379**	-0.385**	0.362**		0.446**	0.41**
LPI_Build	0.247**		0.14**	0.2**	-0.067**		0.082	0.05
SHAPE_MN_Build	-0.048**		0.024	0.02	0.031*		-0.011	-0.003
COHESION_Build	-0.081**		0.016	0.091**	0.075**		-0.005	0.012
PD_Tree	-0.028		-0.016	-0.046	-0.236**		-0.097*	-0.066
ED_Tree	-0.175**		-0.097	-0.03	0.518**		0.248**	0.164**
LPI_Tree	-0.1**		-0.39**	-0.432**	-0.53**		-0.151*	-0.11*
SHAPE_MN_Tree	-0.009		-0.026	-0.049	-0.115**		-0.009	-0.016
COHESION_Tree	-0.153**		0.029	0.027	-0.005		-0.071	-0.053

** denotes the significance of regression coefficient at 0.01 level (2-tailed)* represents the significance at 0.05 level (2-tailed)

time and nighttime LSTs (Fig. 5 (a) and Fig. 6 (a)). Therefore, a more suitable analytical method is required.

Comparing the model performances of RIM and RCM

To measure the degree of heterogeneity in the LST amongst the road-based blocks, the ZM was established to calculate the ICC. In this study, the ICC values were used to quantify the proportion of the total variation in the pixel-level temperature explained by the differences between level-2 blocks. The ICC values of daytime LST and nighttime LST were 35% and 49.4%, respectively, supporting the introduction of level-2 block effects. Therefore, we built two types of multilevel regression models (i.e., RIM and RCM) to explore how block-level variables influence the relationships between pixel-level factors and LST. In this study, the major differences between the RIM and RCM were two-fold: on the one hand, random slope variables in the RCM were involved in further explaining the residual of block level compared to the RIM. On the other hand, the RCM could simultaneously assess the fixed and random effects of random slope variables on LST at the block level. In this section, we focused on investigating the fixed effect of the RCM, the random effects of the RCM were discussed in Section 4.2.

First, we examined the response of pixel-level LST to landscape pattern and 3D urban morphology. As shown in Figs. 3 and 4, the AIC and RMSE values of multilevel models with landscape pattern and 3D urban morphology were smaller than those of multilevel models with only landscape pattern, for both daytime and nighttime LSTs. Moreover, we found similar results for the Moran's I values for the residuals at both the pixel and block levels (Tables 2 and 3). This means that adding the 3D urban morphology variables as pixel-level predictors improved the performance of both the RIM and the RCM. Next, we examined the impacts of buildings and trees on the LST with the RIM and the RCM, depending on the landscape pattern and 3D urban morphology.

During the day, the AIC and RMSE values of the RIM were 70874 and 1.45, respectively. We constructed the RCM for daytime LST by introducing four significant random slope variables: PER_Build, PER_Tree, maximum building height (BH_Max) and BH_Mean. Lower AIC and RMSE values, suggesting a better model fit, were obtained by the RCM, compared to the RIM. The changes in AIC and RMSE values underscored that the block-level variety in the effects of explanatory variables on LST could not be ignored. The residuals of the RIM ranged from -9.89 to 10.62 at the pixel level (Fig. 5 (c)), whereas a narrower residual range (from -9.45 to 8.35) was observed for the RCM (Fig. 5 (d)). The residuals in the block level showed the same conclusion (Fig. 7 (c) and (e)). Furthermore, regardless of pixel level or block level, the Moran's I values of the residuals from the RCM were lower than those of the RIM, suggesting that the residuals provided by the RCM were more random (Table 2). As shown in Table 4, the results from the RIM model showed that the impacts of AREA_SD_BT and SHDI_BT on daytime LST were significant, but these two factors were no longer significantly correlated with daytime LST when the random effects of the level-1 influencing factors were introduced. In contrast, the inclusion of such random effects changed the impact of COHESION_Build on LST from insignificant to significant.

At night, six significant random slope variables (i.e., PER_Build, PER_Tree, BH_Max, BH_Mean, normalized variance of building height (NBH_SD), and TH_Mean) were entered into the RCM. The AIC and RMSE values demonstrated the better suitability of the RCM than the RIM for explaining the hierarchical structure (Fig. 3 (b) and Fig. 4 (b)). At the pixel level, although the RIM and the RCM performed comparably in the residual range, the Moran's I value of the residual from the RCM was smaller than that of the RIM. In contrast, at the block level, the residuals of the RIM ranged from -3.48 to 3.64 (Fig. 7 (d)), and the residuals of the RCM ranged from -2.71 to 2.70 (Fig. 7 (f)). Interestingly, Moran's I value for the block-level residual was higher for the RCM than for the RIM. This means that the RCM explained more residuals of the level-2 blocks, but it failed to reduce the spatial autocorrelation within the block-

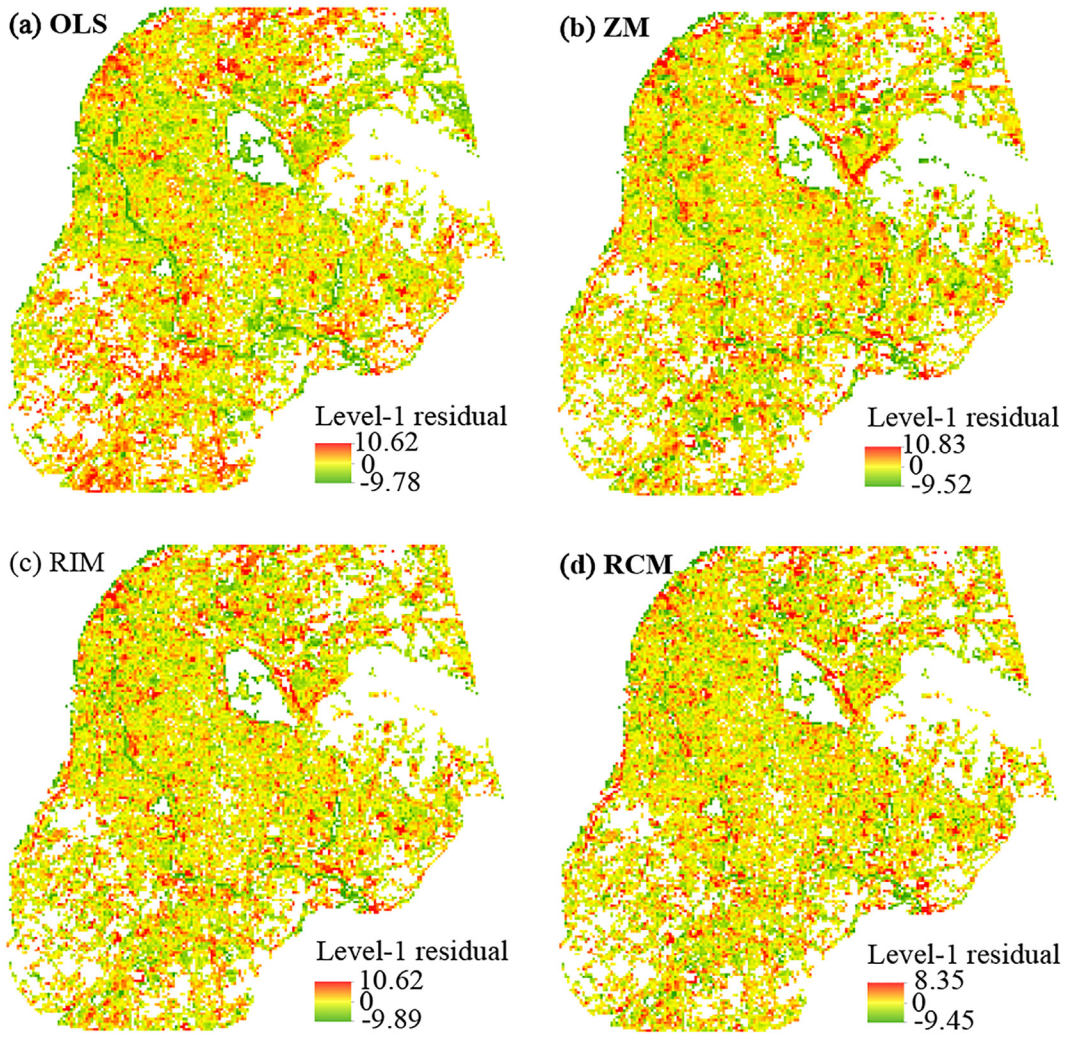

Fig. 5. The spatial distribution of level-1 residual for four regressed models during the day.

level residuals. In addition, the relationship between independent variables and nighttime LST did not vary significantly between the RIM and the RCM (Table 4).

Comparison between single-level and multilevel regression models

Based on the aforementioned results, we concluded that, independent of single-level and multilevel models, combining the landscape pattern and 3D urban morphology produced more precise estimates of the effects of landscape on LST compared to using a single type of urban morphology. Consequently, the comparison between single-level and multilevel models was based on both landscape pattern and 3D urban morphology variables.

As the RCM outperformed the RIM in explaining the variation in LST for both day and night, we used the RCM as the multilevel model to compare single-level OLS regression in quantifying the effects of landscape pattern and 3D urban morphology on LST. For both daytime and nighttime LSTs, we found three major differences in the comparison of OLS and RCM. First, as shown in Figs. 3 and 4, a better fitting result was achieved by the RCM compared to OLS indicated by its much lower AIC and RMSE values. Second, smaller residual ranges were presented by the RCM than OLS, and the Moran's I value indicated that the RCM provided reduced spatial autocorrelation of the residuals. For instance, during the day, the residuals produced by the RCM ranged from -9.45 to 8.35 at the pixel-level (Fig. 5 (d)), but the residuals range of OLS ranged from -9.78 to 10.62 (Fig. 5 (a)). Finally, the RCM allowed for not only the individual impacts of pixels, but also the aggregation impacts of blocks. Therefore, the RCM should more accurately clarify the influences of explanatory variables on LST, in terms of significance and magnitude.In particular, Table 4 demonstrates that OLS showed that PER_Build was the most important predictor of daytime LST. In contrast, the RCM's standardized coefficient estimates demonstrated that PER_Tree most affected the daytime LST, and AREA_SD_BT and SHDI_BT were no longer significantly associated with daytime LST. At night, the most important determinative variable of nighttime LST changed from LPI_Tree to ED_Build with the inclusion of block effects.

Discussion

Relationships between landscape and LST from multilevel and multidimensional perspectives

With an accurate spatial pattern and the vertical structure information of buildings and trees, we used multilevel models to uncover the hierarchical impacts of landscape pattern and 3D urban morphology on LST. Our findings demonstrated that, regardless of daytime or nighttime, not only did pixel-level metrics (i.e.,

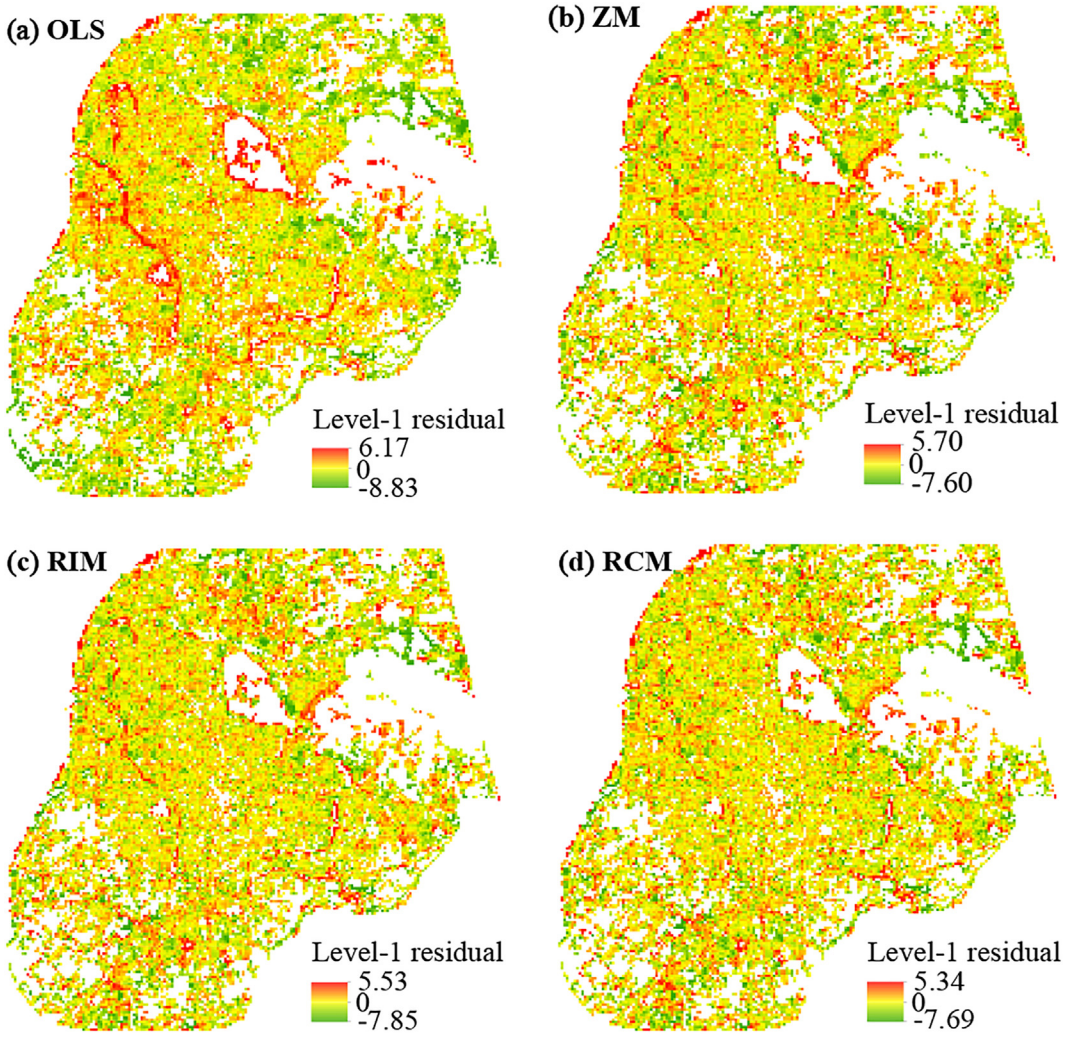

Fig. 6. The spatial distribution of level-1 residual for four regressed models at night.

Table 3
Residual Moran's I of four regressed models for nighttime LST.

Model		Residual Moran's *I*		SD of the residuals	
		Level-1	Level-2	Level-1	Level-2
Regression models with landscape pattern	OLS	0.443**		1.460	
	ZM	0.190**	0.381**	1.083	1.008
	RIM	0.189**	0.257**	1.072	0.841
	RCM	0.175**	0.285**	1.028	0.807
Regression models with landscape pattern and 3D urban morphology	OLS	0.366**		1.357	
	ZM	0.190**	0.381**	1.083	1.008
	RIM	0.176**	0.207**	1.054	0.721
	RCM	0.155**	0.241**	0.981	0.654

** represents the significance at 0.01 level (2-tailed)

composition and 3D urban morphology) significantly influence LST, but also the block-level variables (i.e., configuration).

During the day, the results of Pearson correlation analysis, OLS and RIM models all implied that PER_Tree and PER_Build had stronger associations with LST (Fig. 10 and Table 4), which is consistent with the results of previous studies ([11,62]). For example, Sun et al. ([22]) reported that PER_Build was an important contributor to the UHI effect among all 2D and 3D building structure metrics at the neighborhood scale. However, with the inclusion of the random effects of pixel-level independent variables, the RCM model in this study showed that the relative importance of PER_Build was reduced, and PER_Tree was the most important factor influencing daytime LST, followed by LPI_Tree. These results contrast with those of previous studies ([36,37,54]), which suggested that configuration provided a stronger contribution than composition to the daytime LST. This could be because these studies failed to allow for the multilevel and multi-dimensional effects of urban landscapes on LST.

In this study, we found that PER_Tree played the most important role in mitigating daytime LST. Furthermore, some configura-

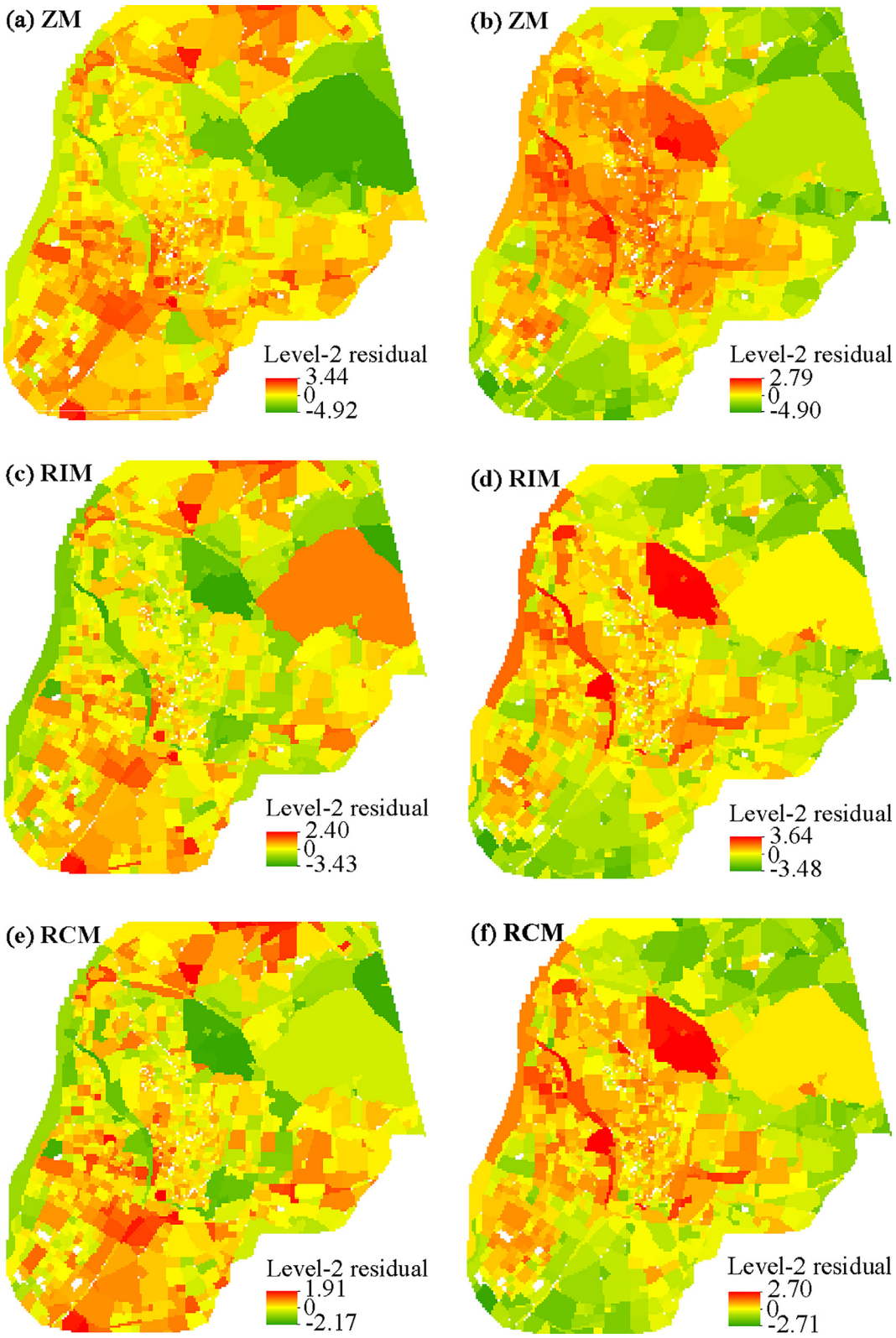

Fig. 7. The spatial distribution of level-2 residual for multilevel regression models. (a), (c) and (e) represent the level-2 residual maps of ZM, RIM and RCM during the day, respectively. The level-2 residual maps of ZM, RIM and RCM at night are shown in (b), (d) and (f), respectively.

tion and 3D urban morphology metrics, such as LPI_Tree, ED_Build and BH_Mean, can also provide cooling effects, which is consistent with findings reported in previous studies ([18,30]). The cooling effect of an increase in ED_Build benefits from the increased energy exchange between the building and surrounding areas such as vegetation ([18]). The reason for the increase in building height resulting in lower LST is mainly because taller buildings produce more shadows ([51]). This result contrasts the findings of the study

conducted in Berlin and Cologne, which have a humid continental climate and temperate oceanic climate, respectively ([63]), and suggested that the effect of building height on LST may rely on the background climate ([64]).

At night, both the Pearson correlation analysis and single-level OLS model suggested that BH_Mean was the most important factor affecting variations in LST (Fig. 10 and Table 4). However, ED_Build was the most influential from the results of multilevel models. These results contrast with those of some previous studies ([31,65]). For instance, a study conducted in four cites in the contiguous United States reported that tree canopy cover dominated LST variation at night ([31]). Furthermore, in our study, by adding the random effects of level-1 explanatory variables to the RIM, the relationship between BH_Mean and nighttime LST strengthened. The increase in nighttime LST was mostly attributed to the increases in ED_Build and BH_Mean. As for ED_Build, given a fixed total quantity of building cover, an increase in ED_Build was always accompanied by a more fragmented building cover. As a

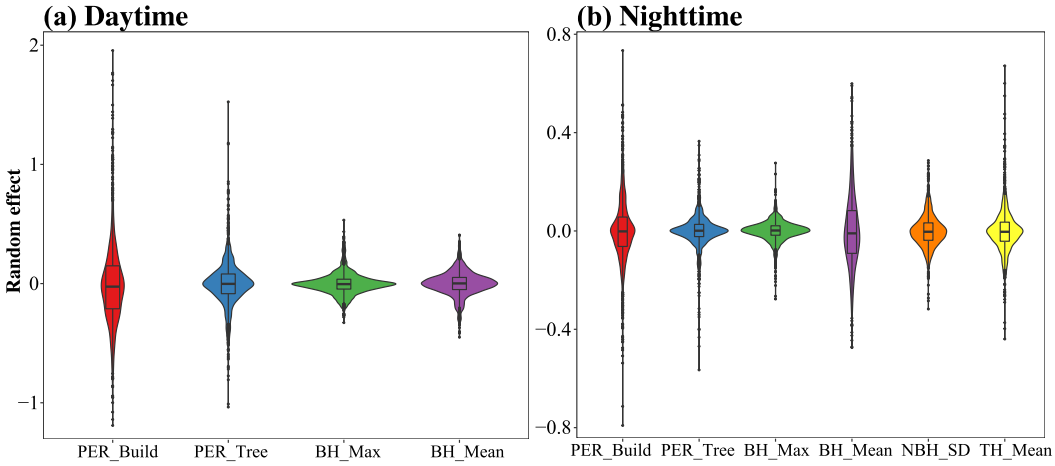

Fig. 8. Violin plot of the random effects of influencing factors for both day and night.

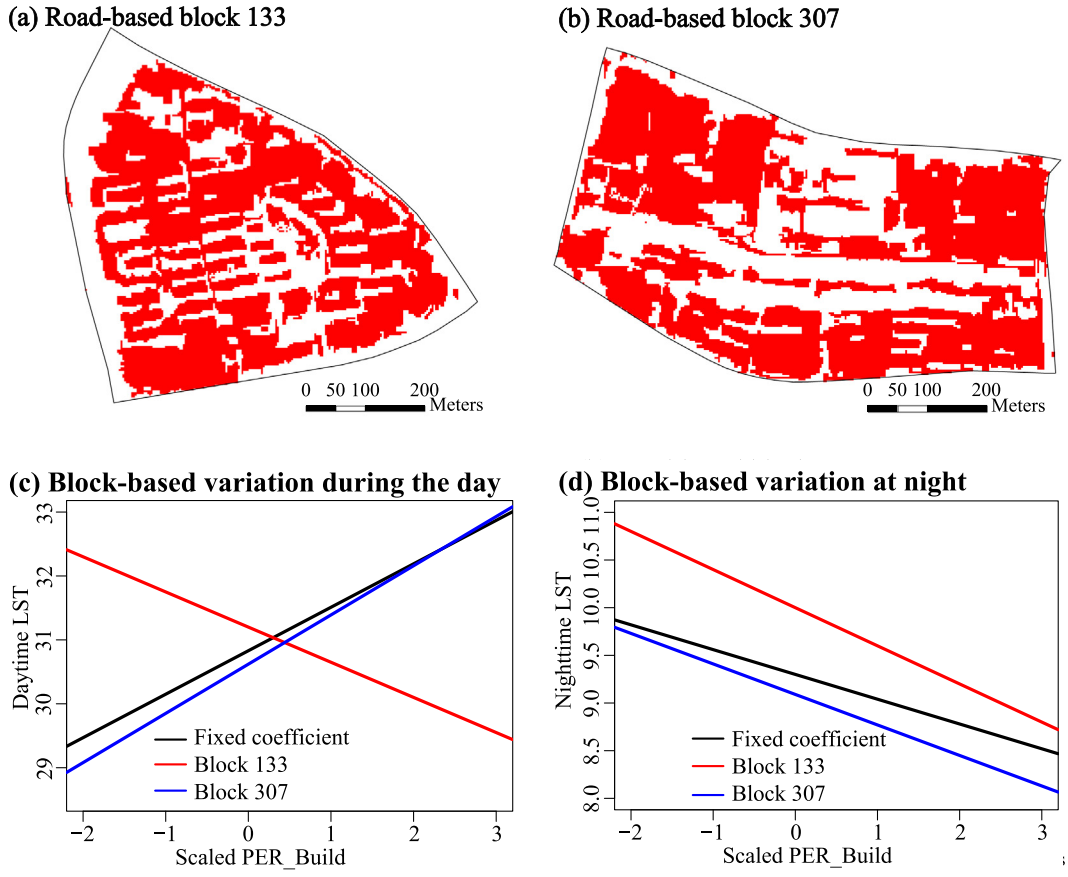

Fig. 9. The urban block variation in the effect of PER_Build on the daytime and nighttime LSTs. Red and blue lines indicated the impacts of PER_Build on LST for block 133 and 307, respectively.

result, this could lead to more exposed surfaces storing solar energy during the day ([66]) and releasing it to elevate nighttime LST, which is consistent with the findings of a previous study ([67]). The warming impact of BH_Mean at night is likely in part because a higher BH_Mean can create urban canyons, trapping more of the released heat ([68]). Furthermore, it is interesting that landscape composition variables (PER_Build and PER_Tree) functioned as the two main landscape features to cool nighttime LST, and PER_Build had a stronger cooling effect than PER_Tree. This can be explained by two aspects: higher PER_Build could enhance the roughness of urban land, and therefore improve the convection efficiency ([69]); because the photosynthesis of urban trees stops at night, their evapotranspirative cooling effect decreases ([70]). These findings provide insights into the importance of considering multidimensional influencing factors along with their multilevel structure and to guide decision making to improve the urban thermal environment.

Urban block-level variety in the impacts of composition and 3D urban morphology on LST

Using the results of the RCM, we investigated how the responses of pixel-level variables to LST varied across urban blocks. The random effects of the pixel-level influencing factors were calculated using Eqs. (8)–(10), and the results described the differences in the mechanism of the UHI among the different blocks. The distributions, which are related to the random effects of composition and 3D urban morphology metrics across urban blocks, are shown in Fig. 8. From Fig. 8 (a) that, we concluded that, during the day, the random effect distributions of 3D urban morphology variables (i.e., BH_Max and BH_Mean) were more compact than those of the composition metrics (i.e., PER_ Build and PER_Tree). This means that BH_Max and BH_Mean demonstrated a relatively small range and degree of random effect fluctuation. The random effect of PER_Tree fluctuated to some extent, but not as much as that of PER_Build. At night, we found a similar result that the random effect of PER_Build varied most across urban blocks (Fig. 8 (b)). The random effect of BH_Mean was distinguished by large variation, which was distinct between day and night. In contrast, BH_Max and NBH_SD showed a low degree of fluctuation for the random effects across urban blocks.

An exemplary study of urban block variation in the impact of scaled PER_Build on LST using our random coefficient model is presented in Fig. 9. The other explanatory variables were set at their average values (i.e., scaled values = 0). Urban blocks 133 and 137 had similar amounts of building cover, which were 44.0% and 41.5%, respectively. However, the distribution of buildings was significantly different. The building cover in block 133 was much more dispersed than that in block 307. During the day, PER_Build was positively related to LST for block 307, but an increase in PER_Build led to a decrease in LST in block 133. This was mainly due to the higher building height and building density in block 133 ([18,30]). This finding suggested that the impact of PER_Build on LST was affected by other factors. Conversely, PER_Build was negatively associated with nighttime LST for both blocks 133 and 307, independent of cooling intensity.

Implications for urban management

The findings of this research demonstrated that LST variation can be driven by both level-1 impacts of composition and 3D urban morphology (pixels) and level-2 impacts of configuration (urban blocks), and that effective strategies to mitigate excess urban heat should vary diurnally.

During the day, when planning tree management, increasing the tree canopy ratio could provide more cooler refugia. We also found that the optimization of the spatial configuration of urban landscapes can enhance their mitigating effects. With the same tree canopy cover area, a single large tree canopy patch had a better cooling effect than small tree canopy patches. Increasing the edge density of building patches, which is usually a consequence of more fragmented building patches given a fixed area of building surface, will result in lower daytime LST. However, at night, we found that decreasing the edge density of building patches was the most effective means of alleviating the UHI effect. The design of the mean building height should also be considered. Low-rise buildings tend to cool the nighttime LST. Furthermore, as the random effect of mean building height varied widely across urban blocks at night, the rational layout and coverage of low-rise buildings would be preferred in urban blocks due to having stronger impacts on nighttime LST.

Limitations and directions of future research

This study's findings provide a detailed understanding of how buildings and trees impact urban warming from multilevel and multi-dimensional perspectives. Nevertheless, this study has some limitations. First, further research should consider the anthropogenic heat emissions, which indirectly exacerbate the UHI effect. For instance, nighttime light data can be considered as a substitute for anthropogenic heat emissions ([71,11,72]). Second, another limitation was due to the lack of considering the meteorological conditions, such as wind speed and wind direction ([73,74]). More studies should be conducted to understand how meteorological conditions affect the relationships between urban landscapes and LST. Third, it is necessary to consider how to adapt the knowledge of UHI mitigation from the micro-scale to the regional scale. For example, the impacts of building and tree shadow patterns on the urban thermal environment should be examined in the further studies ([27]). Fourth, with the availability of high-resolution thermal data, we want to provide a precise analysis of the impacts of 2D and 3D characteristics of urban landscapes on LST and identify the mechanism underlying urban landscape-LST relationships with respect to different tree species and urban functional zones ([75–79]).Finally, more cities in different climatic zones can be considered for evaluating the generalizability of our findings based on 3D information on a large scale ([69,67]).

Conclusions

Although previous studies have attempted to evaluate the multilevel effects of landscape pattern on daytime LST, it was not previously clear how landscape pattern and 3D urban morphology hierarchically interact to impact diurnal LST. Therefore, this study will contribute to a deeper understanding about how diurnal LST can be explained by the level-1 impacts of composition and 3D urban morphology (pixel-level) and level-2 effects of configuration (urban block-level). Our results implied that, regardless of single-level OLS and multilevel models, the model performance can be enhanced significantly with the addition of 3D urban morphology. By adding the 3D urban morphology to the RCM model with the landscape pattern, AIC values decreased by 999.3 and 1277 for day and night, respectively. Multilevel models performed better than OLS in capturing the effects of urban landscapes on daytime and nighttime LSTs. In addition, compared to the RIM, the RCM achieved a better fit because of the incorporation of the local effects of the composition and 3D urban morphology variables. During the day, the standard deviation of the residual and autocor-

relation in the residuals for the RCM were 1.315 and 0.131, respectively, but were separately 1.715 and 0.312 for OLS. Similarly, smaller standard deviation of the residual and autocorrelation in the residual were generated by RCM than by OLS. The findings of the RCM showed that the most important factors influencing daytime LST were PER_Tree and LPI_Tree, and ED_Build and BH_Mean most affected nighttime LST. Another interesting aspect was that the increase in daytime LST was mostly determined by PER_Build, whereas PER_Build had the maximum cooling effect on LST at night. Moreover, we found that the random effect of PER_Build on LST varied more across urban blocks for day and night than that of the other composition and 3D urban morphology variables. BH_Mean was more variable at night than during the day, in terms of its random effect. This study's findings not only underscore the importance of considering the multi-dimensional characteristics of land cover but also provides new insights into the multilevel effects of the factors driving the urban thermal environment.

Declaration of Competing Interest

The authors declare that they have no known competing financial interests or personal relationships that could have appeared to influence the work reported in this paper.

Acknowledgements

This work is supported by Project funded by the National Natural Science Foundation of China (No. 42101354, 41871028); Strategic Priority Research Program Project of the Chinese Academy of Sciences (Grant No. XDA23040100); and China Postdoctoral Science Foundation (No. 2019M661885).

Appendix

Fig. 10

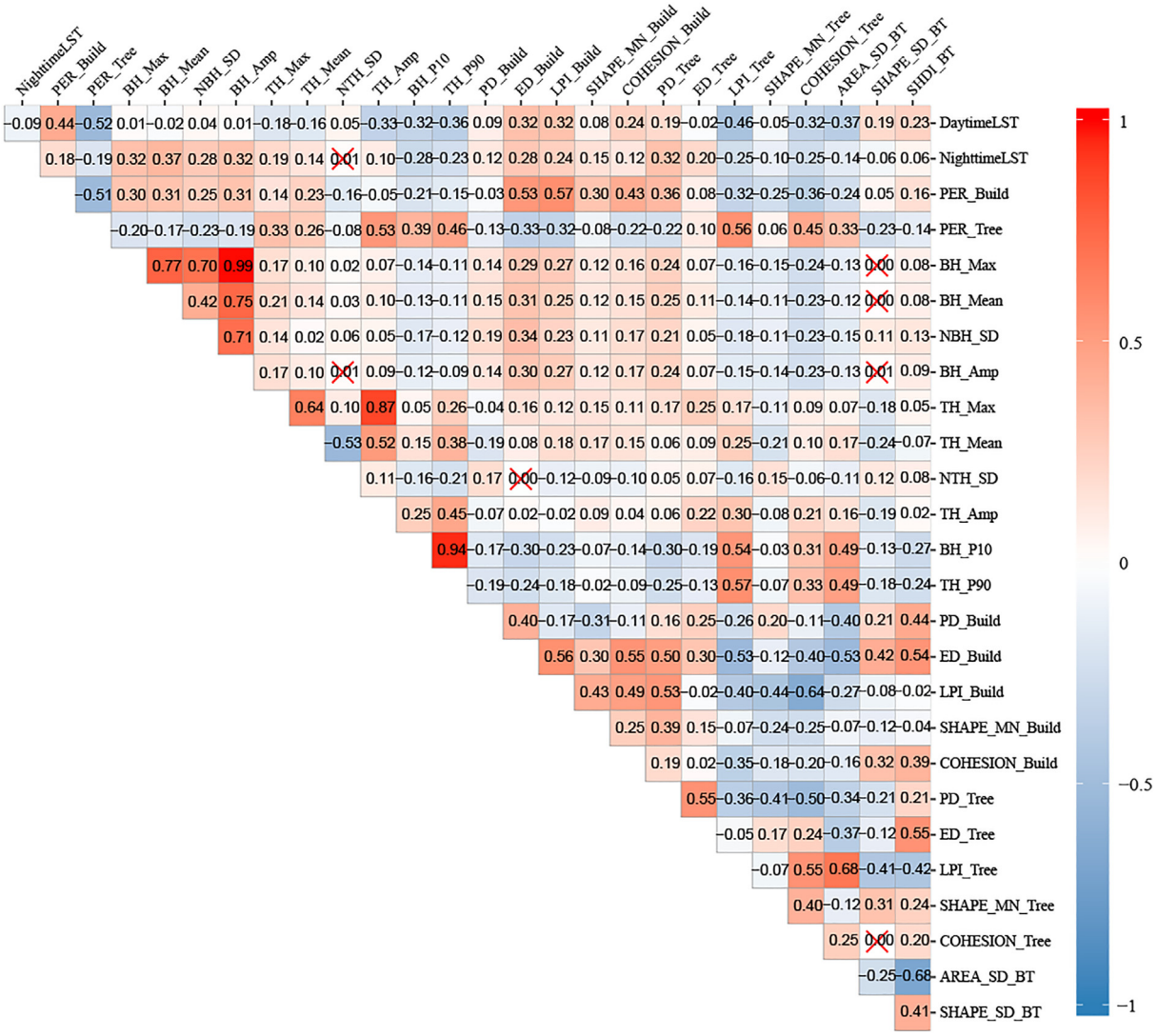

Fig. 10. Pearson correlation coefficients between LST and independent variables, together with between independent variables for both day and night. Correlation coefficient insignificant (p>0.05) was labeled with red cross. The descriptions of all the abbreviations used are shown in Table 1.

References

[1] P.M. Vitousek, H.A. Mooney, J. Lubchenco, J.M. Melillo, Human domination of earth's ecosystems, Science 277 (5325) (1997) 494–499.
[2] N.B. Grimm, S.H. Faeth, N.E. Golubiewski, C.L. Redman, J. Wu, X. Bai, J.M. Briggs, Global change and the ecology of cities, Science 319 (5864) (2008) 756–760.
[3] T.R. Oke, City size and the urban heat island, Atmospheric Environment (1967) 7 (8) (1973) 769–779..
[4] R. Watkins, J. Palmer, M. Kolokotroni, Increased temperature and intensification of the urban heat island: Implications for human comfort and urban design, Built Environment 33 (1) (2007) 85–96.
[5] H. Akbari, M. Pomerantz, H. Taha, Cool surfaces and shade trees to reduce energy use and improve air quality in urban areas, Solar Energy 70 (3) (2001) 295–310.
[6] Y. Vitasse, C. Signarbieux, Y.H. Fu, Global warming leads to more uniform spring phenology across elevations, Proceedings of the National Academy of Sciences 115 (5) (2018) 1004–1008.
[7] L. Meng, Y. Zhou, X. Li, G.R. Asrar, J. Mao, A.D. Wanamaker Jr, Y. Wang, Divergent responses of spring phenology to daytime and nighttime warming, Agricultural and Forest Meteorology 281 (2020) 107832.
[8] A.J. McMichael, R.E. Woodruff, S. Hales, Climate change and human health: present and future risks, The Lancet 367 (9513) (2006) 859–869.
[9] R. Amiri, Q. Weng, A. Alimohammadi, S.K. Alavipanah, Spatial–temporal dynamics of land surface temperature in relation to fractional vegetation cover and land use/cover in the Tabriz urban area, Iran, Remote Sensing of Environment 113 (12) (2009) 2606–2617.
[10] A. Buyantuyev, J. Wu, Urban heat islands and landscape heterogeneity: linking spatiotemporal variations in surface temperatures to land-cover and socioeconomic patterns, Landscape Ecology 25 (1) (2010) 17–33.
[11] J. Peng, J. Jia, Y. Liu, H. Li, J. Wu, Seasonal contrast of the dominant factors for spatial distribution of land surface temperature in urban areas, Remote Sensing of Environment 215 (2018) 255–267.
[12] F. Yuan, M.E. Bauer, Comparison of impervious surface area and normalized difference vegetation index as indicators of surface urban heat island effects in Landsat imagery, Remote Sensing of Environment 106 (3) (2007) 375–386.
[13] F. Kong, H. Yin, P. James, L.R. Hutyra, H.S. He, Effects of spatial pattern of greenspace on urban cooling in a large metropolitan area of eastern China, Landscape and Urban Planning 128 (2014) 35–47.
[14] O. Soydan, Effects of landscape composition and patterns on land surface temperature: Urban heat island case study for Nigde, Turkey, Urban Climate 34 (2020) 100688.
[15] K. McGarigal, Landscape pattern metrics, Wiley StatsRef: Statistics Reference Online..
[16] W. Zhou, J. Wang, M.L. Cadenasso, Effects of the spatial configuration of trees on urban heat mitigation: A comparative study, Remote Sensing of Environment 195 (2017) 1–12.
[17] J. Chen, S. Jin, P. Du, Roles of horizontal and vertical tree canopy structure in mitigating daytime and nighttime urban heat island effects, International Journal of Applied Earth Observation and Geoinformation 89 (2020) 102060.
[18] W. Zhou, G. Huang, M.L. Cadenasso, Does spatial configuration matter?, Understanding the effects of land cover pattern on land surface temperature in urban landscapes, Landscape and Urban Planning 102 (1) (2011) 54–63
[19] J. Li, C. Song, L. Cao, F. Zhu, X. Meng, J. Wu, Impacts of landscape structure on surface urban heat islands: A case study of Shanghai, China, Remote Sensing of Environment 115 (12) (2011) 3249–3263.
[20] J. Rhee, S. Park, Z. Lu, Relationship between land cover patterns and surface temperature in urban areas, GIScience & Remote Sensing 51 (5) (2014) 521–536.
[21] M. Scarano, J. Sobrino, On the relationship between the sky view factor and the land surface temperature derived by Landsat-8 images in Bari, Italy, International Journal of Remote Sensing 36 (19–20) (2015) 4820–4835.
[22] F. Sun, M. Liu, Y. Wang, H. Wang, Y. Che, The effects of 3D architectural patterns on the urban surface temperature at a neighborhood scale: Relative contributions and marginal effects, Journal of Cleaner Production 258 (2020) 120706.
[23] Q. Yu, M. Acheampong, R. Pu, S.M. Landry, W. Ji, T. Dahigamuwa, Assessing effects of urban vegetation height on land surface temperature in the City of Tampa, Florida, USA, International Journal of Applied Earth Observation and Geoinformation 73 (2018) 712–720.
[24] G. Li, Z. Ren, C. Zhan, Sky view factor-based correlation of landscape morphology and the thermal environment of street canyons: A case study of Harbin, china, Building and Environment 169 (2020) 106587.
[25] X. Yang, Y. Li, The impact of building density and building height heterogeneity on average urban albedo and street surface temperature, Building and Environment 90 (2015) 146–156.
[26] T.E. Morakinyo, W. Ouyang, K.K.-L. Lau, C. Ren, E. Ng, Right tree, right place (urban canyon): Tree species selection approach for optimum urban heat mitigation-development and evaluation, Science of the Total Environment 719 (2020) 137461.
[27] F. Lindberg, C. Grimmond, The influence of vegetation and building morphology on shadow patterns and mean radiant temperatures in urban areas: model development and evaluation, Theoretical and Applied Climatology 105 (3–4) (2011) 311–323.
[28] C. Yin, M. Yuan, Y. Lu, Y. Huang, Y. Liu, Effects of urban form on the urban heat island effect based on spatial regression model, Science of the Total Environment 634 (2018) 696–704.
[29] C. Alexander, Influence of the proportion, height and proximity of vegetation and buildings on urban land surface temperature, International Journal of Applied Earth Observation and Geoinformation 95 (2021) 102265.
[30] X. Huang, Y. Wang, Investigating the effects of 3D urban morphology on the surface urban heat island effect in urban functional zones by using high-resolution remote sensing data: A case study of Wuhan, Central China, ISPRS Journal of Photogrammetry and Remote Sensing 152 (2019) 119–131.
[31] T. Logan, B. Zaitchik, S. Guikema, A. Nisbet, Night and day: The influence and relative importance of urban characteristics on remotely sensed land surface temperature, Remote Sensing of Environment 247 (2020) 111861.
[32] S. Alavipanah, J. Schreyer, D. Haase, T. Lakes, S. Qureshi, The effect of multi-dimensional indicators on urban thermal conditions, Journal of Cleaner Production 177 (2018) 115–123.
[33] J. Niemelä, Is there a need for a theory of urban ecology?, Urban Ecosystems 3 (1) (1999) 57–65
[34] J. Wu, Hierarchy and scaling: extrapolating information along a scaling ladder, Canadian Journal of Remote Sensing 25 (4) (1999) 367–380.
[35] R.A. Berk, J. De Leeuw, Multilevel statistical models and ecological scaling, in: Scaling and uncertainty analysis in ecology, Springer, 2006, pp. 67–88..
[36] S. Du, Z. Xiong, Y.-C. Wang, L. Guo, Quantifying the multilevel effects of landscape composition and configuration on land surface temperature, Remote Sensing of Environment 178 (2016) 84–92.
[37] C.S. Greene, P.J. Kedron, Beyond fractional coverage: A multilevel approach to analyzing the impact of urban tree canopy structure on surface urban heat islands, Applied Geography 95 (2018) 45–53.
[38] Z. Tong, Y. Chen, A. Malkawi, Defining the influence region in neighborhood-scale cfd simulations for natural ventilation design, Applied Energy 182 (2016) 625–633.
[39] M. Lotteau, P. Loubet, M. Pousse, E. Dufrasnes, G. Sonnemann, Critical review of life cycle assessment (lca) for the built environment at the neighborhood scale, Building and Environment 93 (2015) 165–178.
[40] R. Kellett, A. Christen, N.C. Coops, M. van der Laan, B. Crawford, T.R. Tooke, I. Olchovski, A systems approach to carbon cycling and emissions modeling at an urban neighborhood scale, Landscape and Urban Planning 110 (2013) 48–58.
[41] R. Sun, Y. Lü, L. Chen, L. Yang, A. Chen, Assessing the stability of annual temperatures for different urban functional zones, Building and Environment 65 (2013) 90–98.
[42] J. Song, W. Chen, J. Zhang, K. Huang, B. Hou, A.V. Prishchepov, Effects of building density on land surface temperature in China: Spatial patterns and determinants, Landscape and Urban Planning 198 (2020) 103794.
[43] L. Yao, T. Li, M. Xu, Y. Xu, How the landscape features of urban green space impact seasonal land surface temperatures at a city-block-scale: An urban heat island study in Beijing, China, Urban Forestry & Urban Greening 52 (2020) 126704.
[44] F. Kong, H. Yin, C. Wang, G. Cavan, P. James, A satellite image-based analysis of factors contributing to the green-space cool island intensity on a city scale, Urban Forestry & Urban Greening 13 (4) (2014) 846–853.
[45] W. Qiao, Y. Liu, Y. Wang, B. Fang, Y. Zhao, The relationship of evolution between urban land use types and intensity in Nanjing since the early 21st century, Acta Geographica Sinica 70 (11) (2015) 1800–1810.
[46] Y. Sun, M. Pu, B. Zhang, L. Yao, M. Liu, Analysis of high temperature days anomaly in nanjing, Scientia Meteorologic Sinica 30 (2) (2010) 279–284.
[47] A. Gillespie, S. Rokugawa, T. Matsunaga, J.S. Cothern, S. Hook, A.B. Kahle, A temperature and emissivity separation algorithm for advanced spaceborne thermal emission and reflection radiometer (ASTER) images, IEEE Transactions on Geoscience and Remote Sensing 36 (4) (1998) 1113–1126.
[48] M. Abrams, The Advanced Spaceborne Thermal Emission and Reflection Radiometer (ASTER): data products for the high spatial resolution imager on NASA's Terra platform, International Journal of Remote Sensing 21 (5) (2000) 847–859.
[49] M. Scarano, F. Mancini, Assessing the relationship between sky view factor and land surface temperature to the spatial resolution, International Journal of Remote Sensing 38 (23) (2017) 6910–6929.
[50] F.-Y. Gong, Z.-C. Zeng, F. Zhang, X. Li, E. Ng, L.K. Norford, Mapping sky, tree, and building view factors of street canyons in a high-density urban environment, Building and Environment 134 (2018) 155–167.
[51] A.K. Nassar, G.A. Blackburn, J.D. Whyatt, Dynamics and controls of urban heat sink and island phenomena in a desert city: Development of a local climate zone scheme using remotely-sensed inputs, International Journal of Applied Earth Observation and Geoinformation 51 (2016) 76–90.
[52] J.J. Arsanjani, A. Zipf, P. Mooney, M. Helbich, An introduction to openstreetmap in geographic information science: Experiences, research, and applications, in: OpenStreetMap in GIScience, Springer, 2015, pp. 1–15.
[53] A. Chen, L. Yao, R. Sun, L. Chen, How many metrics are required to identify the effects of the landscape pattern on land surface temperature?, Ecological Indicators 45 (2014) 424–433
[54] X. Li, W. Li, A. Middel, S. Harlan, A. Brazel, B. Turner Ii, Remote sensing of the surface urban heat island and land architecture in Phoenix, Arizona: Combined effects of land composition and configuration and cadastral–demographic–economic factors, Remote Sensing of Environment 174 (2016) 233–243.
[55] Y. Chen, S. Yu, Impacts of urban landscape patterns on urban thermal variations in Guangzhou, China, International Journal of Applied Earth Observation and Geoinformation 54 (2017) 65–71.
[56] S. Shi, H. Li, X. Ding, X. Gao, Effects of household features on residential window opening behaviors: A multilevel logistic regression study, Building and Environment 170 (2020) 106610.

[57] C. Li, Y. Song, N. Kaza, Urban form and household electricity consumption: A multilevel study, Energy and Buildings 158 (2018) 181–193.
[58] M. Brauer, J.J. Curtin, Linear mixed-effects models and the analysis of nonindependent data: A unified framework to analyze categorical and continuous independent variables that vary within-subjects and/or within-items, Psychological Methods 23 (3) (2018) 389.
[59] M. Masoudi, P.Y. Tan, Multi-year comparison of the effects of spatial pattern of urban green spaces on urban land surface temperature, Landscape and Urban Planning 184 (2019) 44–58.
[60] S. Nakagawa, H. Schielzeth, A general and simple method for obtaining R^2 from generalized linear mixed-effects models, Methods in Ecology and Evolution 4 (2) (2013) 133–142.
[61] P.A. Moran, The interpretation of statistical maps, Journal of the Royal Statistical Society, Series B (Methodological) 10 (2) (1948) 243–251.
[62] B. Yuan, L. Zhou, X. Dang, D. Sun, F. Hu, H. Mu, Separate and combined effects of 3d building features and urban green space on land surface temperature, Journal of Environmental Management 295 (2021) 113116.
[63] C. Berger, J. Rosentreter, M. Voltersen, C. Baumgart, C. Schmullius, S. Hese, Spatio-temporal analysis of the relationship between 2D/3D urban site characteristics and land surface temperature, Remote Sensing of Environment 193 (2017) 225–243.
[64] L. Zhao, X. Lee, R.B. Smith, K. Oleson, Strong contributions of local background climate to urban heat islands, Nature 511 (7508) (2014) 216.
[65] A. Dewan, G. Kiselev, D. Botje, Diurnal and seasonal trends and associated determinants of surface urban heat islands in large bangladesh cities, Applied Geography 135 (2021) 102533.
[66] J.A. Voogt, T. Oke, Effects of urban surface geometry on remotely-sensed surface temperature, International Journal of Remote Sensing 19 (5) (1998) 895–920.
[67] C. Wang, Y. Li, S.W. Myint, Q. Zhao, E.A. Wentz, Impacts of spatial clustering of urban land cover on land surface temperature across köppen climate zones in the contiguous United States, Landscape and Urban Planning 192 (2019) 103668.
[68] A.J. Arnfield, C. Grimmond, An urban canyon energy budget model and its application to urban storage heat flux modeling, Energy and Buildings 27 (1) (1998) 61–68.
[69] L. Zhao, X. Lee, R.B. Smith, K. Oleson, Strong contributions of local background climate to urban heat islands, Nature 511 (7508) (2014) 216–219.
[70] C.D. Ziter, E.J. Pedersen, C.J. Kucharik, M.G. Turner, Scale-dependent interactions between tree canopy cover and impervious surfaces reduce daytime urban heat during summer, Proceedings of the National Academy of Sciences (2019) 201817561..
[71] S. Peng, S. Piao, P. Ciais, P. Friedlingstein, C. Ottle, F.-M. Bréon, H. Nan, L. Zhou, R.B. Myneni, Surface urban heat island across 419 global big cities, Environmental Science & Technology 46 (2) (2012) 696–703.
[72] G. Molnár, A. Kovács, T. Gál, How does anthropogenic heating affect the thermal environment in a medium-sized Central European city?, A case study in Szeged, Hungary, Urban Climate 34 (2020) 100673
[73] J. Konarska, B. Holmer, F. Lindberg, S. Thorsson, Influence of vegetation and building geometry on the spatial variations of air temperature and cooling rates in a high-latitude city, International Journal of Climatology 36 (5) (2016) 2379–2395.
[74] B.-J. He, Potentials of meteorological characteristics and synoptic conditions to mitigate urban heat island effects, Urban Climate 24 (2018) 26–33.
[75] M.A. Irmak, S. Yilmaz, E. Mutlu, H. Yilmaz, Assessment of the effects of different tree species on urban microclimate, Environmental Science and Pollution Research 25 (16) (2018) 15802–15822.
[76] S. Leuzinger, R. Vogt, C. Körner, Tree surface temperature in an urban environment, Agricultural and Forest Meteorology 150 (1) (2010) 56–62.
[77] M. Irmak, S. Yİlmaz, H. Yİlmaz, S. Ozer, S. Toy, et al., Evaluation of different thermal conditions based on thi under different kind of tree types-as a specific case in ata botanic garden in eastern Turkey., Global NEST Journal 15 (1) (2013) 131–139..
[78] P.J. Trowbridge, N.L. Bassuk, Trees in the urban landscape: site assessment, design, and installation, John Wiley & Sons, 2004.
[79] Z. Tan, K.K.-L. Lau, E. Ng, Planning strategies for roadside tree planting and outdoor comfort enhancement in subtropical high-density urban areas, Building and Environment 120 (2017) 93–109.